ISSN: 2476-6909; Modares. Mech. Eng. *2026;26(12):935-947.*

Modares Mechanical Engineering

DOI: 10.48311/mme.2026.117984.82899
journal homepage: mme.modares.ac.ir

Developing a Graphical User Interface Background Named SUT-AUVSIM for the AUV Maneuverability Analysis

Ali Hasanvand[1]*, Mohammad Saeed Seif[2]

[1]Maritime Engineering Department, Khorramshahr University of Maritime and Technology, Khorramshahr, Iran
[2]Mechanical Engineering Department, Sharif University of Technology, Tehran, Iran

ARTICLE INFO

Article Type
Original Research

Article History
Received: November 30, 2025
Revised: January 29, 2026
Accepted: February 18, 2026
ePublished: September 17, 2026

ABSTRACT

The design and maneuvering analysis of Autonomous Underwater Vehicles (AUVs) typically require multiple independent tools, resulting in time-consuming and inefficient workflows. To address this limitation, this research introduces SUT-AUVSIM, a novel graphical user interface that integrates hydrodynamic body design, derivative estimation, and maneuvering simulation within a single framework, significantly reducing the overall analysis time from several months to a few minutes. The software enables users to design C-type AUV hulls based on DARPA classes, Series 58, Myring, and DRDC configurations, which are not simultaneously supported in existing tools. Once the body is designed, SUT-AUVSIM estimates the hydrodynamic derivatives of the main body and appendages using strip theory. The algorithm includes a database of control surface profiles, such as NACA 0009, 0012, 0015, and elliptic sections, to facilitate design flexibility. After computing the derivatives, the software simulates traditional marine maneuvers, including turning, descending, and helical motions. The simulation results are exported as a *.txt* file, containing data such as position, velocities, Euler angles, and effective angles of attack for the appendages. The maneuver parameters are generated quickly, allowing users to evaluate the impact of hydrodynamic parameters on the maneuverability of AUVs. This capability makes SUT-AUVSIM a valuable tool for optimizing AUV designs and improving their performance in real-world scenarios.

Keywords: SUT-AUVSIM, Maneuverability, GUI, Torpedo Shape, Strip Theory

How to cite this article
Hasanvand A, Seif M.S, Developing a Graphical User Interface Background Named SUT-AUVSIM for the AUV Maneuverability Analysis. Modares Mechanical Engineering; *2026;26(12):935-947.*

**Corresponding author's email:ali.hsnvd@gmail.com*
**Corresponding ORCID ID: 0000-0001-7912-9613*

شاپا: ۷۶۰۹-۲۴۷۶؛ مهندسی مکانیک مدرس. ۹۴۷-۹۳۵:(۱۲)۲۶;۱٤۰۵

مهندسی مکانیک مدرس

DOI: 10.48311/mme.2026.117984.82899

صفحه اصلی مجله: mme.modares.ac.ir

توسعه رابط کاربری با عنوان SUT-AUVSIM برای تحلیل مانورپذیری ربات های AUV

علی حسنوند[۱]*، محمد سعید سیف[۲]

[۱] گروه مهندسی دریا، دانشگاه علوم وفنون دریایی، خرمشهر، ایران
[۲] گروه مهندسی دریا، دانشگاه صنعتی شریف، تهران، ایران

اطلاعات مقاله

نوع مقاله
مقاله پژوهشی

تاریخچه مقاله
دریافت: ۱۴۰۴/۰۹/۰۹
بازنگری: ۱۴۰۴/۱۱/۰۹
پذیرش: ۱۴۰۴/۱۱/۲۹
ارائه آنلاین: ۱۴۰۵/۰۶/۲۶

چکیده

طراحی و تحلیل مانورپذیری ربات‌های AUV معمولاً مستلزم استفاده از چندین ابزار مستقل است که این امر منجر به فرآیندهای تحلیلی زمان‌بر می‌شود. به‌منظور رفع این محدودیت، در این پژوهش SUT-AUVSIM به‌عنوان یک رابط کاربری مناسب ارائه شده است که طراحی هیدرودینامیکی بدنه، تخمین مشتقات هیدرودینامیکی و شبیه‌سازی مانور را در یک چارچوب یکپارچه گرد هم می‌آورد و زمان کلی تحلیل را از بصورت چشم گیری کاهش می‌دهد. این برنامه امکان طراحی بدنهAUV های نوع C را بر اساس پیکربندی‌هایDARPA ، سری ۵۸، Myringو DRDC فراهم می‌کند؛ پیکربندی‌هایی که به‌صورت هم‌زمان در ابزارهای موجود پشتیبانی نمی‌شوند. پس از طراحی بدنه، برنامه با استفاده از تئوری نواری، مشتقات هیدرودینامیکی بدنه اصلی و سطوح کنترلی را تخمین می‌زند. همچنین، در درون الگوریتم توسعه داده شده، دیتاهایی از پروفیل‌های سطوح کنترلی پرکاربرد، از جمله NACA 0009، NACA 0012، NACA 0015و مقاطع بیضوی موجود است که انعطاف‌پذیری بیشتری را در طراحی فراهم می‌کند.

کلیدواژه‌ها: SUT-AUVSIM، مانورپذیری، تئوری نواری، بدنه Torpedo

نحوه ارجاع به این مقاله
حسنوند علی، سیف محمد سعید، توسعه رابط کاربری با عنوان SUT-AUVSIM برای تحلیل مانورپذیری ربات های AUV، مهندسی مکانیک مدرس. ۹٤۷-۹۳۵:(۱۲)۲٦;۱٤۰۵

*پست الکترونیکی نویسنده عهده‌دار مکاتبات: ali.hsnvd@gmail.com
*شناسه ارکید نویسنده عهده‌دار مکاتبات: ۰۰۰۰-۰۰۰۱-۷۹۱۲-۹٦۱۳

1- Introduction

Numerous studies in engineering, biology, commerce, and military fields related to open water have consistently captured the interest of researchers. Therefore, the expansion of maritime industries and marine sciences has become crucial for addressing a wide range of applications, including the exploration and extraction of underwater resources, environmental monitoring, and data collection, as well as the installation, repair, and maintenance of coastal and offshore structures. Such activities demand specialized technologies to cover the ever-growing demands [1]. Autonomous Underwater Vehicles are among the advanced technologies utilized worldwide for research and operational purposes, such as ocean exploration, performing various industrial operations, or military missions [2].

The design, manufacturing, and dynamics are substantial aspects of any AUV. The forces and moments exerted on the hull by the surrounding fluid are significantly influenced by its shape and curvature. Additionally, the pressure distribution on the hull and the velocity field are other critical aspects affected by the hull shape. Myring et al. introduced a specific hull form to obtain an optimal balance between enclosed volume and drag, while also evaluating the impact of nose and tail curvatures on drag coefficients. Because of the direct effect on drag, the hull shape is a crucial character, as it significantly influences energy consumption and restricts the endurance range.

The body and appendages of an AUV play the main role in determining the pattern of the flow field characteristics, pressure distribution, and boundary layer around the vehicle. In contrast, an AUV's control system is implemented based on dynamic behaviors and stability analyses, which are essential components for developing an effective control system [3]. Extensive research has been conducted on the dynamic modeling and behavior analysis of AUVs. Mackay experimentally investigated the forces and moments acting on the DRDC series body using a wind tunnel. The strip theory method has been applied to estimate added mass derivatives and damping coefficients for AUVs [4, 5]. Eng et al. utilized the WAMIT™ software to estimate added mass coefficients and damping ratios for an ROV [6]. Furthermore, Fossen developed a six-degree-of-freedom dynamic model that incorporates restoring forces, damping, and environmental disturbances, providing a robust framework for the dynamic modeling of underwater marine vehicles with hydrodynamic coefficients [7].

Strip theory is a traditional and effective method for estimating hydrodynamic coefficients and dynamic modeling of AUVs. This approach, based on potential flow theory, provides satisfactory results for simple shapes with insignificant curvature and moderate vehicle velocities. However, this method does not account for the surge velocity of the vehicle in the calculation of hydrodynamic coefficients. For AUVs with simple body shapes and relatively low surge velocities, strip theory remains a practical and suitable approach [8]. Gutnik et al. employed strip theory to estimate the added mass and damping coefficients of the ALICE AUV, enabling the development of an appropriate model for designing a path-following control system under various conditions [9]. Strip theory, by aiding in the dynamic modeling of underwater robots, can be applied to parametric studies of underwater vehicles such as underwater gliders and performance evaluations. Specifically, the evaluation of the diving motion and kinematics of underwater gliders are critical aspects where strip theory has proven to be a practical tool [10]. Beyond strip theory, advanced methods have also been employed for trajectory estimation and dynamic modeling of AUVs. These methods often rely on experimental free-run test results to estimate hydrodynamic coefficients [11].

System identification methods based on experimental tests have been widely used to calculate hydrodynamic derivatives. For instance, recursive least squares and prediction error methods for offline and online identification of AUV dynamics was applied [12], and system identification with optimal input design to estimate hydrodynamic coefficients of an AUV model have been employed in [13].

Additionally, computational fluid dynamics (CFD) methods have emerged as a novel approach for studying the flow regime around the body and fins of AUVs [14]. CFD method can be applied to the flow study around quadrotors [15].

Recent developments in the hydrodynamic analysis of AUVs have increasingly leveraged CFD-based techniques to improve the accuracy of flow predictions around complex hull geometries, addressing limitations of traditional lower-order methods in capturing detailed pressure and wake characteristics [16]. A comprehensive survey on CFD-based hydrodynamic performance investigation highlights not only advanced numerical methods such as RANS and hybrid turbulence models, but also their practical applications in hull shape optimization [17]. Furthermore, reviews of subsea AUV technologies emphasize the role of modern computational methods—including CFD and semi-analytical approaches—in addressing complex flow regimes and the trade-offs between accuracy and computational cost [18].

The design and maneuvering analysis of Autonomous Underwater Vehicles (AUVs) typically require multiple independent tools, resulting in time-consuming and inefficient workflows. To address this limitation, this research introduces SUT-AUVSIM, a novel graphical user interface that integrates hydrodynamic body design, derivative estimation, and maneuvering simulation within a single framework. The developed GUI incorporates nonlinear six-degree-of-freedom modeling, significantly reducing calculation time and addressing this gap identified in previous research. The application provides a user-friendly workspace that allows users to design an AUV body within four classes of practical geometry based on user-defined inputs. Furthermore, the GUI can compute hydrodynamic coefficients and simulate various maneuvers, including turning, descending, and helical maneuvers, under open water currents. By developing this algorithm, the software significantly reduces the computational burden on users, making it an efficient tool for AUV design and analysis.

2- Mathematical modeling

Mathematical dynamic modeling is utilized to predict the behavior of underwater robots. These models are not only used for behavior prediction but also for designing control and path-following systems. Having an efficient six-degree-of-freedom dynamic model enhances control system efficiency, reduces costs, and ultimately extends endurance range. Some approaches have been applied to AUV modeling, among which the use of hydrodynamic derivatives to estimate the forces and moments acting on the vehicle is one of the most conventional and precise methods. To estimate forces through hydrodynamic derivatives, it is necessary to define a coordinate system on the body that fixed to the body. However, certain states, such as the vehicle's position, cannot be meaningfully defined in a movable coordinate system. Dynamic modeling typically involves two coordinate systems: one fixed to the Earth as an inertial reference frame and the other fixed to the vehicle’s body. The body-fixed coordinate system is often assumed to be located at the center of buoyancy. Figure 1 illustrates the relative configuration of the coordinate systems considered for the modeling process.

The notations used in modeling and simulations for six-degree-of-freedom motions follow the standard marine vehicle notation, as shown in Table 1.

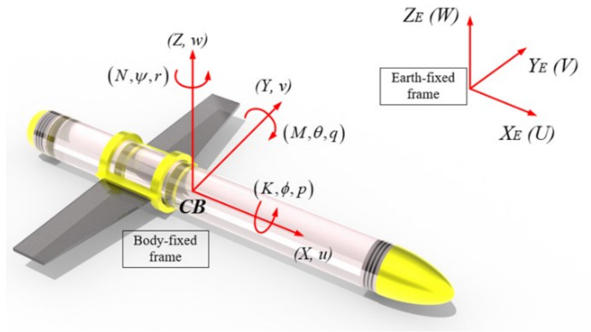

Fig. 1 Coordinate systems defined for dynamic modeling [3]

Table 1 Notations used for motion modeling [3]

Number	Description	Position and Euler angles	Linear and angular velocities	Forces and moments
1	Move along x axis (surge)	x	u	X
2	Move along y axis (sway)	y	v	Y
3	Move along z axis (heave)	z	w	Z
4	Move around x axis (roll)	ϕ	p	K
5	Move around y axis (pitch)	θ	q	M
6	Move around z axis (yaw)	ψ	r	N

2-1- Kinematic of rigid body

The position must be defined in the Earth-fixed coordinate system and the user's perspective. Therefore, for this purpose, linear velocities are converted from the body-fixed coordinate system to the Earth-fixed coordinate system using kinematic equations. Subsequently, by integrating the converted velocities, the vehicle's position can be calculated. All motions in space can be described by the vectors presented in Equation (1).

$$\begin{aligned} \eta_1 &= [\ x \quad y \quad z\ ]^T; & \eta_2 &= [\ \phi \quad \theta \quad \psi\ ]^T \\ v_1 &= [\ u \quad v \quad w\ ]^T; & v_2 &= [\ p \quad q \quad r\ ]^T \\ \tau_1 &= [\ X \quad Y \quad Z\ ]^T; & \tau_2 &= [\ K \quad M \quad N\ ]^T \end{aligned} \tag{1}$$

Here, η describes the position and orientation relative to the Earth-fixed frame, $\boldsymbol{v}$ represents the translational and rotational velocities in the body-fixed frame, and $\boldsymbol{\tau}$ denotes the total forces and moments acting on the body. To transform the translational velocities between the body-fixed frame and the Earth-fixed frame, the transformation matrix provided in Equation (2) is used.

$$\dot{\eta}_1 = J_1(\eta_2)v_1, \quad \dot{\eta}_2 = J_2(\eta_2)v_2 \tag{2}$$

Here, $J_1(\eta_2)$ and $J_2(\eta_2)$ are the transformation matrix, which is a function based on the Euler angles, as indicated in Equation (3).

$$\begin{aligned} J_1(\eta_2) &= \begin{bmatrix} c\psi\, c\theta & -s\psi\, c\phi + c\psi\, s\theta\, s\phi & s\psi\, s\phi + c\psi\, s\theta\, c\phi \\ s\psi\, c\theta & c\psi\, c\phi + s\psi\, s\theta\, s\phi & -c\psi\, s\phi + s\psi\, s\theta\, c\phi \\ -s\theta & s\phi\, c\theta & c\phi\, c\theta \end{bmatrix} \\ J_2(\eta_2) &= \begin{bmatrix} 1 & t\theta s\phi & t\theta c\phi \\ 0 & c\phi & -s\phi \\ 0 & s\phi/c\theta & c\phi/c\theta \end{bmatrix} \end{aligned} \tag{3}$$

In Equation (3), for simplicity, ***sin(.) = s(.)*** and ***cos(.) = c(.)*** are used. After calculating the translational velocities in the Earth-fixed frame, the position is determined by integrating, as indicated in Equation (4).

$$\eta_i{}^t = \int_0^t \left(\dot{\eta}_i{}^t + \dot{\eta}_i{}^{t-\Delta t}\right)/2\, dt + \eta_i{}^0 \tag{4}$$

In Equation (4), t represents the simulation time, and Δt is the simulation time step.

2-2- Dynamic of AUV

The six-degree-of-freedom dynamic model of the AUV is presented in this section. A dynamic model is a mathematical model framework that estimates the trajectory and states by determining the forces and moments acting on the body, allowing the evaluation of the vehicle's response and stability based on the actuator inputs. The nonlinear mathematical model in Equation (5) has been used for modeling AUVs and UGs in several studies, which be derived from the Newton-Euler equation of motion, as indicated in Equation (5) [3, 7, 8].

$$M_{RB}\dot{v} + C_{RB}(v)v + M_A\dot{v} + C_A(v)v + D(v)v + G(\eta) = \tau_w + \tau_P \tag{5}$$

Here, M represents the mass and inertia term, where "RB" and "A" are related to the rigid body and the hydrodynamic added mass, respectively, $C(v)$ denotes the Coriolis and centrifugal acceleration term, $D(v)$ is the hydrodynamic damping term, $G(\eta)$ is the gravitational and buoyancy acceleration term of the AUV. Additionally, τ_p accounts the propeller effect, τ_w is about the fins, and v is the velocity vector.

An AUV with a torpedo-shaped body, four fins arranged in the C-type configuration, and a marine propeller is typically symmetry in the xz and xy planes. By assuming a symmetric body, the rigid body equations for an AUV can be derived, as in Equation (6).

$$\begin{aligned} (m + m_{11})\dot{u} &= \sum X_{ext} \\ (m + m_{22})\dot{v} + m_{26}\dot{r} &= \sum Y_{ext} \\ (m + m_{33})\dot{w} + m_{35}\dot{q} &= \sum Z_{ext} \\ (I_{xx} + m_{44})\dot{p} &= \sum K_{ext} \\ (I_{yy} + m_{55})\dot{q} + m_{53}\dot{w} &= \sum M_{ext} \\ (I_{zz} + m_{66})\dot{r} + m_{62}\dot{v} &= \sum N_{ext} \end{aligned} \tag{6}$$

Here, m represents the mass, I denotes the inertia tensor, and m_{ij} refers to the hydrodynamic added mass terms. The effect of added mass can be modeled as a linear term, as indicated in Equation (6). However, the added mass terms are highly dependent on the body shape. When the AUV is fully submerged, the added mass coefficients can be assumed to be constant and linear behavior, exhibiting linear behavior.

2-3- Coriolis and centripetal terms

$C(v)$ consists of two terms: $C_{RB}(v)$ and $C_A(v)$. $C_{RB}(v)$ is the Coriolis and centrifugal acceleration term related to the M_{RB} term, while $C_A(v)$ is associated with the M_A term. In Equation (7), the general form of the $C_{RB}(v)$ is indicated, and in Equation (8), the $C_A(v)$ is presented.

$$C_{RB}(v) = \begin{bmatrix} 0 & 0 & 0 & 0 & -mw & mv \\ 0 & 0 & 0 & mw & 0 & -mu \\ 0 & 0 & 0 & -mv & mu & 0 \\ 0 & -mw & mv & 0 & I_{zz}r & -I_{yy}q \\ mw & 0 & mu & -I_{zz}r & 0 & I_{xx}p \\ -mv & -mu & 0 & I_{yy}q & -I_{xx}p & 0 \end{bmatrix} \tag{7}$$

$$C_A(v) = \begin{bmatrix} 0 & 0 & 0 & 0 & -a_3 & a_2 \\ 0 & 0 & 0 & a_3 & 0 & -a_1 \\ 0 & 0 & 0 & -a_2 & a_1 & 0 \\ 0 & -a_3 & a_2 & 0 & -b_3 & b_2 \\ a_3 & 0 & -a_1 & b_3 & 0 & -b_1 \\ -a_2 & a_1 & 0 & -b_2 & b_1 & 0 \end{bmatrix} \tag{8}$$

The parameters in Equation (8) are explained in Table 2 via the added mass coefficients for the cross-flow body. For the case when the body-fixed coordinate system, as shown in Figure 1, is located at the center of buoyancy, the values of y_g and x_g are insignificant, then the rigid body equations for symmetrical bodies are derived as Equation (9-10).

Table 2 Parameters of the $C_A(v)$ for symmetrical body AUVs

Parameter	Description	Parameter	Description
a_1	$m_{11}u$	b_1	$m_{44}p$
a_2	$m_{22}v + m_{26}r$	b_2	$m_{35}w + m_{55}q$
a_3	$m_{33}w + m_{35}q$	b_3	$m_{66}r + m_{26}v$

$$\begin{aligned} m[\dot{u} - vr + wq + z_g(pr + \dot{q})] &= \sum X_{ext} \\ m[\dot{v} - wp + ur + z_g(qr - \dot{p})] &= \sum Y_{ext} \\ m[\dot{w} - uq + vp - z_g(p^2 + q^2)] &= \sum Z_{ext} \end{aligned} \tag{9}$$

$$\begin{aligned} I_{xx}\dot{p} + (I_{zz} - I_{yy})qr - m[z_g(\dot{v} - wp + ur)] &= \sum K_{ext} \\ I_{yy}\dot{q} + (I_{xx} - I_{zz})rp + m[z_g(\dot{u} - vr + wq)] &= \sum M_{ext} \\ I_{zz}\dot{r} + (I_{yy} - I_{xx})pq &= \sum N_{ext} \end{aligned} \tag{10}$$

2-4- Damping terms

The hydrodynamic damping represents the drag and lift forces acting on an AUV moving underwater. However, for a low-level speed AUV, lift forces are insignificant compared to the drag force. Drag forces can be classified into two different forms: a linear term and a quadratic term, based on Equation (11) [19].

$$D = D_L + D_Q \tag{11}$$

Here, D_L and D_Q represent the linear and quadratic damping terms, respectively.

2-5- Restoring term

The weight and buoyancy values, along with their positions, determine the static forces on the AUV. The hydrostatic forces and moments in six degrees of freedom based on Euler angles and $\Delta B = W - B$ for these robots are indicated in Equation (12) [20].

$$G(\eta) = \begin{bmatrix} -\Delta B s\theta & \Delta B s\phi c\theta & \Delta B c\phi c\theta & W z_g s\phi c\theta & W z_g s\theta & 0 \end{bmatrix}^T \tag{12}$$

2-6- Propeller effects

Marine propellers are traditionally the propulsion system for AUVs. These rotating appendages, operating in the submerged condition, create a pressure differential, and the resulting thrust force is generated from this pressure difference. The performance of a marine propeller depends on its hydrodynamic coefficients, the most important of which is its thrust coefficient. A semi-empirical relation for the thrust force of the propeller is given by Equation (13).

$$\tau_P = K_T \rho n^2 D^4 \tag{13}$$

Where n is the rotational velocity of the propeller, D is the maximum diameter of the propeller, and K_T is the thrust coefficient, which can be estimated using the polynomial versus advance coefficient in Equation (14).

$$K_T = k_0 + k_1 J + k_2 J^2 \tag{14}$$

Where J is the advance coefficient of the propeller. Finally, the general form of the motion equations is derived [20].

3- Environmental disturbances

To model the forces and moments induced by ocean currents on the AUV, the motion equation can be rewritten as Equation (15). To consider the effects of ocean currents, the relative velocity between the AUV and the current is incorporated into the equations of motion. This relative velocity is used in the added mass and hydrodynamic damping terms to model environmental disturbances [7].

$$\{M_{RB}\dot{v} + C_{RB}(v)v + G(\eta)\} + \{M_A\dot{v}_r + C_A(v_r)v_r + D(v_r)v_r\} = \tau_w + \tau_P \tag{15}$$

The left side of the equation corresponds to the rigid body and hydrostatic forces, while the right side represents the hydrodynamic forces. The relative velocity vector is defined as $v_r = v - v_c$, where v_c is the induced current velocity. The relative velocities affect only the linear velocities of the AUV and have an insignificant impact on the angular velocities. To compute the relative velocity, the ocean current velocities must be defined in the body-fixed frame by Equation (16).

$$v_c = [V_c c\zeta c\theta \quad V_c(s\zeta c\phi + c\zeta s\theta s\phi) \quad V_c(c\zeta s\theta + s\zeta s\phi) \quad 0 \quad 0 \quad 0]^T \tag{16}$$

V_c represents the current velocity, and ζ denotes the direction of the current relative to the AUV's heading, as indicated in Equation (17).

$$\zeta = \beta_c - \psi \tag{17}$$

β_c is the current direction relative to the North, with a range of $[-\pi, \pi]$. The relative angle between the heading and the current direction is defined in Figure 2.

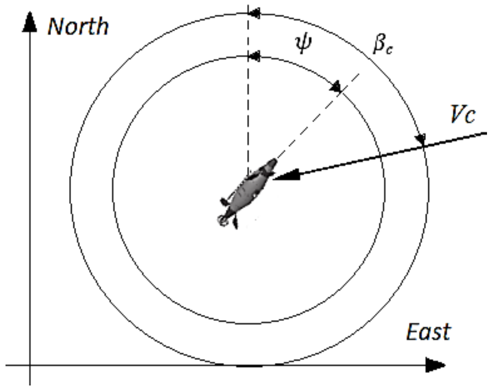

Fig. 2 Relative angle between the AUV's heading and the direction of ocean currents

4- Hydrodynamic derivations

4-1- Added mass

In this study, the strip theory method has been used to calculate the hydrodynamic derivations for the body and fins. This theory computes the unknown terms and hydrodynamic derivatives over two-dimensional sections. The hydrodynamic derivatives are derived using strip theory, which assumes negligible surge velocity effects. While this assumption is generally valid for low-speed maneuvers, it may become less accurate for high-speed scenarios or complex geometries, where non-linear flow effects become more pronounced. A validation of the results against CFD benchmarks for the selected hull classes would provide further insight into the accuracy of the assumption and help assess potential discrepancies in maneuvering at higher velocities or in curved paths. Due to the low-level velocities of AUVs in six-DOF and the uncomplicated shape of the two-dimensional sections of the body, the strip theory provides appropriate results of the coefficients. The added mass, damping derivatives, and fin forces are determined using this method. However, the drag and added mass along the surge direction cannot be computed using strip theory alone. Figure 3 indicates the two-dimensional body sections used in the strip theory.

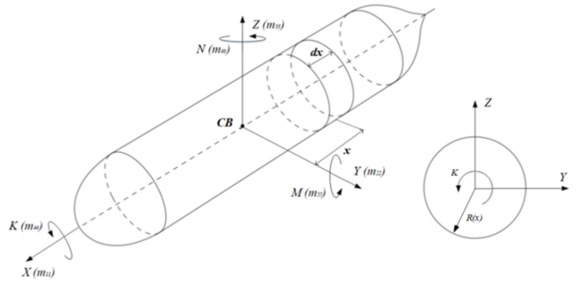

Fig. 3 Cross-sections and two-dimensional sections in strip theory

The two-dimensional sections of the body are generally circular, making the determination of added mass and damping on these sections straightforward. Consequently, the added mass along the axial direction of the two-dimensional sections is obtained using Equation (18).

$$m_a(x) = \pi\rho R(x)^2 \tag{18}$$

Here, *R(x)* is the circular radius of the two-dimensional sections, and ρ is the fluid density. Subsequently, based on the linear theory of the potential flow, the superposition approach is applied to incorporate the added mass and damping of the fins into the body coefficients (Figure 4).

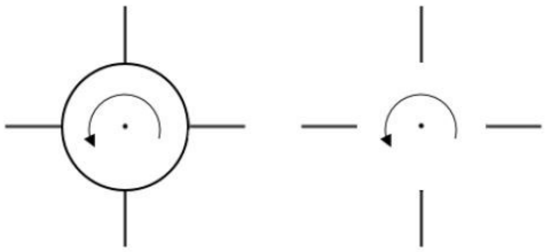

Fig. 4 Superposition of the effect of fins and body sections in strip theory

As shown in Equations (19), by summing the coefficients of all the sections along the length of the body, the three-dimensional translational and rotational coefficients of the body are obtained.

$$m_{ii} = \int_{-l/2}^{l/2} a_{ii}\, dx \tag{19}$$

In this case, *x* represents the longitudinal distance of each section from the center of buoyancy. For other coupling coefficients, the process follows the approach outlined in Equation (20).

$$m_{ij} = \int_{-l/2}^{l/2} x a_{ii}\, dx \tag{20}$$

To calculate the added mass of fins, semi-empirical equations from previous studies can be used (Equations 21).

$$m_{22f} = k_{tr}\frac{\pi\rho c^2 b^3}{4} \quad , \quad m_{22f} = m_{33f} \tag{21}$$

Here, *c* and *b* are the chord and span lengths, and x_f and y_f represent the longitudinal and lateral distances of the appendage from the center of buoyancy. k_{tr} represents the three-dimensional effect of the appendage on the added mass coefficient, which is expressed in Equation (22).

$$k_{tr} = \frac{1}{\sqrt{1+\frac{1}{AR}}} \tag{22}$$

Where *AR* is the fin aspect ratio. The notation used in this research for naming hydrodynamic derivatives follows the SNAME (1950) convention. For instance, the hydrodynamic added mass along the Y-axis due to $\dot{u}$ is expressed in Equation (23). Additionally, Table 3 provides further details on the hydrodynamic derivatives.

$$Y_{\dot{u}} = \frac{\partial Y}{\partial \dot{u}} \quad , \quad Y_{\dot{u}} = m_{21} \tag{23}$$

Table 3 Notations of hydrodynamic coefficients for AUVs

Parameter	Definition
$X_{uu}, X_{\dot{u}}$	Derivation along x axis
$Y_{vv}, Y_{\dot{r}}, Y_{\dot{v}}, Y_{rr}$	Derivation along y axis
$Z_{\dot{w}}, Z_{ww}, Z_{\dot{q}}, Z_{qq}$	Derivation along z axis
$K_{pp}, K_{\dot{p}}$	Derivation around x axis
$M_{ww}, M_{\dot{w}}, M_{\dot{q}}, M_{qq}$	Derivation around y axis
$N_{vv}, N_{\dot{v}}, N_{rr}, N_{\dot{r}}$	Derivation around z axis

4-2- Axial and cross-flow damping

The motion of the AUV's body surrounded by fluid leads to the formation of the boundary layer and vortices around the body. The generated forces as cross-flow drag resist the body's motion in the fluid. The cross-flow drag includes contributions from both the body and fin. Like the calculation of added mass coefficients, the total drag is computed by summing the drag contributions from the two-dimensional body sections. The nonlinear cross-flow drag coefficients are obtained through Equations (24).

$$\begin{aligned} Y_{vv} &= Z_{ww} = -\frac{1}{2}\rho c_d \int_{-l/2}^{l/2} 2R(x)dx \\ M_{ww} &= -N_{rr} = \frac{1}{2}\rho c_d \int_{-l/2}^{l/2} 2xR(x)dx \\ Y_{rr} &= -Z_{qq} = -\frac{1}{2}\rho c_d \int_{-l/2}^{l/2} 2x|x|R(x)dx \\ M_{qq} &= N_{rr} = -\frac{1}{2}\rho c_d \int_{-l/2}^{l/2} 2x^3R(x)dx \end{aligned} \tag{24}$$

Linear damping coefficients are used for better accuracy at low velocities. The linear damping coefficients are roughly determined using an approximation derived from the nonlinear coefficients (Equation (25)).

$$\begin{aligned} Y_v &= Z_w = 0.1\, Y_{vv} \\ M_q &= N_r = 0.2\, M_{qq} \\ K_p &= 5\, K_{pp} \end{aligned} \tag{25}$$

4-3- Fin forces and moments

Most AUVs are equipped with two horizontal surface controls for depth control and two vertical surface controls (rudders) for plane control. The rotation of these fin pairs is usually coordinated. For the control surfaces, the empirical lift coefficient relationship is as shown in Equation (26).

$$\begin{aligned} L_F &= \frac{1}{2}\rho c_L S_F \delta u^2 \\ M_F &= x_f L_F \end{aligned} \tag{26}$$

Where C_L, S_F, and δ are the lift coefficient, area, and effective angle of attack of the control surface, respectively. In Equation (27), the effects of the fin's thickness, aspect ratio, and sweep angle on the lift coefficient are considered. Also, Equation (28) is utilized to obtain the effective angle of attack of the control surface.

$$C_L = \frac{2\pi AR\left[1-3\left(\frac{t}{C}\right)^2\right]}{2.6+\cos\Omega\sqrt{2+\frac{AR^2}{\cos^2\Omega}}}\delta + 2.1\delta^3 \tag{27}$$

$$\begin{aligned} \delta_r &= \xi_r - \beta_r \\ \delta_s &= \xi_s + \beta_s \end{aligned} \tag{28}$$

Where ξ_r and ξ_s are the rudder angle and fin angle relative to the body. β_r and β_s represent the induced angles for the fin and rudder, respectively. The induced angles for the rudder and fin are presented in Equation (29).

$$\beta_r = \tan^{-1}\frac{v + x_f r}{u}$$
$$\beta_s = \tan^{-1}\frac{w - x_f q}{u} \qquad (29)$$

5- Graphical user interface background

To facilitate the maneuvering and dynamic modeling of underwater robots, a MATLAB GUI-based environment has been created, enabling users to quickly obtain desired outputs. This GUI accelerates the design process and enhances the presentation of results. The program, named SUT-AUVSIM, was developed at Sharif University of Technology for modeling descending, turning, and spiral maneuvers under environmental disturbances. SUT-AUVSIM utilizes a six-DOF nonlinear dynamic model, specifically designed for AUVs with a torpedo-shaped body, four fins arranged in a C-type configuration, and an axial thruster.

All algorithms were implemented within the MATLAB GUI environment, and inputs are provided by the user. Figures 5-6 illustrate the perspective view of the initial inputs interface. The GUI models maneuvers based on weight, velocity, depth, maximum fin angle, and propeller diameter, and it supports four different body classes: DARPA, DRDC, Seri 58, and Myring for the designing body. The geometric shape and mathematical equations for these body classes are presented in Table 4. The calculated coefficients, trajectory, and other parameters such as trajectory, velocities, and Euler angles are exported as a *.txt* file.

.

Table 4 Shape and mathematical equations for the body geometry used in the SUT-AUVSIM database

1	Body Seri name	Myring
	Shape	
	Nose eq	$R(x) = \frac{D}{2}\left[1 - \left(\frac{x}{L_{fore}}\right)^2\right]^{\frac{1}{n_f}}$
	Tail eq	$R(x) = \frac{D}{2} - \left[\frac{3D}{2L_{aft}^2} - \frac{\tan\alpha_t}{L_{aft}}\right]x^2 + \left[\frac{D}{L_{aft}^3} - \frac{\tan\alpha_t}{L_{aft}^2}\right]x^3$
2	Body Seri name	DARPA
	Shape	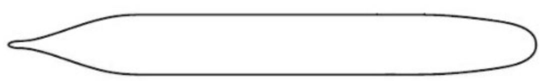
	Nose eq	$R(x) = \frac{D}{2}[1.126395101x(0.3x-1)^4 + 0.442874707x^2\ (0.3x-1)^4(1.2x+1)]^{1/2.1}$
	Tail eq	$R = \frac{D}{2}\Big[r_h^2 + r_h K_0 \varrho^2 + \left(20 - 20r_h^2 - 4r_hK_0 - \frac{1}{3}K_1\right)\varrho^3 + (-45 + 45r_h^2 + 6r_hK_0 + K_1)\varrho^4 + (36 - 36r_h^2 - 4r_hK_0 - K_1)\varrho^5 + \left(-10 + 10r_h^2 + r_hK_0 + \frac{1}{3}K_1\right)\varrho^6\Big]^{1/2}$
		$r_h = 0.1175, \quad K_0 = 10, \quad K_1 = 44.6244, \quad \varrho = \frac{13.979167 - x}{3.3334}$
3	Body Seri name	DRDC
	Shape	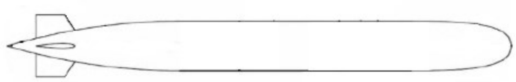
	Nose eq	$\frac{R(x)}{D} = 0.8685\sqrt{\frac{x}{D}} - 0.3978\frac{x}{D} + 0.006511\left(\frac{x}{D}\right)^2 + 0.005086\left(\frac{x}{D}\right)^3$
	Tail eq	$\frac{R(x)}{D} = \frac{1}{3}\left(\frac{x}{D}\right) - \frac{1}{18}\left(\frac{x}{D}\right)^2$
4	Body Seri name	Series 58
	Shape	
	Body eq	$R(x) = a_1x + a_2x^2 + a_3x^3 + a_4x^4 + a_5x^5 + a_6x^6$

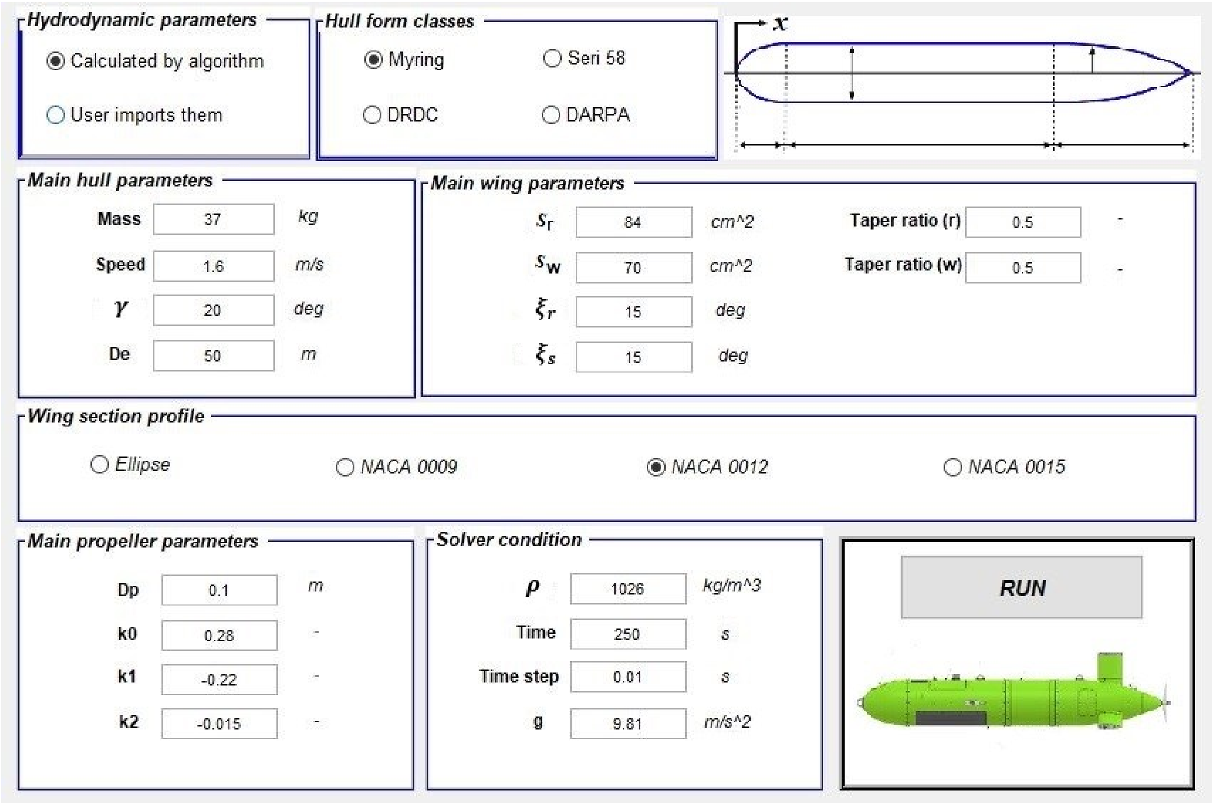

Fig. 5 Snapshot from the SUT-AUVSIM's input sector

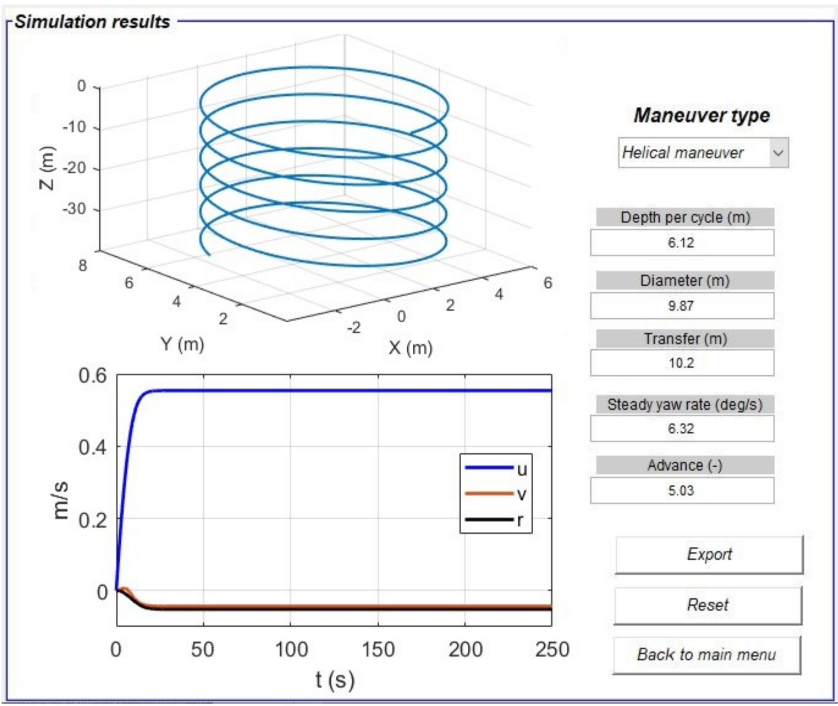

Fig. 6 Snapshot from the SUT-AUVSIM's output sector

5-1- Validation

The results generated by the developed software are evaluated in this section through a comparison with experimental tests and earlier research results to ensure their validity. The SUT-AUVSIM takes user inputs, such as length, diameter, and weight to compute the moment of inertia through the suggested ITTC as indicated in Equations (30).

$$I_{xx} = k_{xx}^2 \, m$$
$$I_{yy} = k_{yy}^2 \, m \tag{30}$$

$I_{zz} = k_{zz}^2 m$

k_{xx}, k_{yy}, and k_{zz} are the gyration radius of the AUV which are calculated using Equations (31).

$$k_{xx} = 0.3\,D \quad k_{yy} = 0.25\,L \quad k_{zz} = 0.25\,L \tag{31}$$

In the validation procedure, the turning maneuver trajectory of an AUV named ARMs1.0 is compared with experimental results [21]. The specifications for modeling are provided in Table 5. The target AUV starts with an initial speed of 1 m/s, moving under its propulsion. When the AUV reaches a steady self-propulsion condition, its rudders are defeated by 10 degrees to initiate the turning maneuver. The forces and moments generated by the rudders induce the yaw rate, resulting in the turning maneuver. If the derivatives are accurately calculated, the simulated maneuver closely matches the experimental results. Figure 7 compares the two approaches for the turning maneuver.
Additionally, a depth-change maneuver test was conducted on the AUV ARMs1.0. The robot initially advances at a speed of 1 m/s at a depth of 0.5 meters. The control system then commands the robot to dive to a depth of 2 meters, where it maintains its course for 60 seconds before returning to 0.5 meters by deflecting its fins at 80 seconds. The diving maneuver to a depth of 2 meters was tested experimentally in the referenced study [21], and the maneuver was re-simulated using the SUT-AUVSIM, indicated in Figure 8.

Table 5 Characteristic of AUV ARMs1.0 [21]

Number	Parameters	Value
1	Length (m)	**1.07**
2	Diameter (m)	**0.14**
3	LtoD	**7.64**
4	Mass (kg)	**7.7**
5	Speed (m/s)	**1**
6	Ruder angle (deg)	**10**

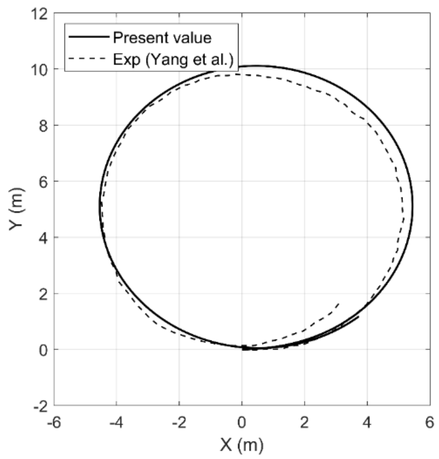

Fig. 7 Comparison of the trajectory of AUV ARMs1.0 turning maneuver in experimental and simulation approach with 10 degrees rudder angle deflection [21]

The results of the turning and depth-change maneuvers indicate that the SUT-AUVSIM adequately simulates the motion and behavior of the AUV ARMs1.0. The error of 11 cm in predicting the turning tactical diameter and the insignificant difference in the diving path highlight the validity and efficiency of the developed software. Furthermore, the algorithm appropriately simulates the dynamics and forces acting on the body, as evidenced by the oscillations around the desired depth in both approaches.

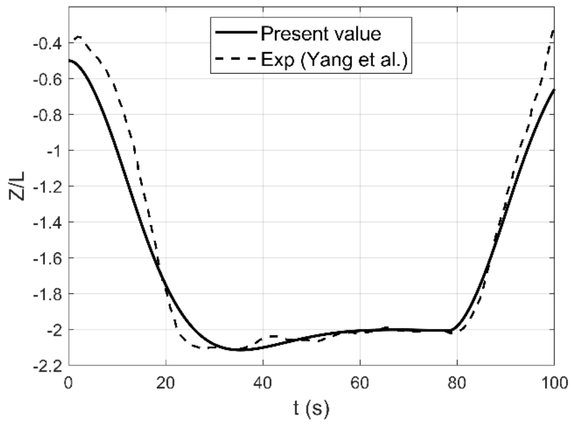

Fig. 8 Comparison of the trajectory of AUV ARMs1.0 descending maneuver in experimental and simulation approach [21]

The coefficients calculated by the SUT-AUVSIM have been compared with the results from previous studies. The hydrodynamic derivatives for the AUV Pirajuba were calculated by software. The geometric specifications of the AUV, including its length, diameter, and mass (1.88 meters, 0.234 meters, and 72.8 kg, respectively), were provided as inputs to the algorithm. For comparison, the hydrodynamic coefficients obtained by Cardenas et al. were derived from real-world tests and system identification methods [22].
Table 6 presents a comparison of the results from the SUT-AUVSIM with the system identification method. As shown in Table 6, the software has adequately estimated several of the coefficients, with computational errors falling within an acceptable range. However, for some derivatives, the error exceeds 100%. This discrepancy arises because the GUI determines the body profile based on the length, diameter, mass, and standard profiles, which may not fully capture the identical body geometry of the AUV Pirajuba. Additionally, in the system identification method, the coefficients are optimized to minimize error, which may exclude the effects of external disturbances that are inherently included in the derivatives.

6- Results and discussion

In this section, the outputs and practical results of the SUT-AUVSIM are reviewed. This section includes the simulation results for three traditional maneuvers for AUVs: turning, descending, and helical maneuvers. Two well-known body profiles, Myring and DARPA, were used for modeling. The inputs were defined in the input section of the SUT-AUVSIM (Figure 5), and outputs such as the trajectory, velocities, and body drift angle were exported in *.txt* format.

6-1- Turning Maneuver

In this maneuver, the AUV moves at the target velocity under self-propulsion conditions and begins turning by deflecting the control surfaces (e.g., rudders) to a specified angle.
For the simulation, the mass was set to 37 kg, the cruise velocity to 1 m/s, and the maximum rudder angle to 15 degrees. Both the Myring and DARPA body geometries were used for the simulations in the SUT-AUVSIM, and the results are shown in Figure 9. The total simulation time is less than 10 seconds, significantly aiding in the rapid assessment of various states to reach an optimal concept design. The maneuver characteristics, including quantitative metrics such as settling times, overshoot percentages, and maximum yaw rates, are presented in Table 7, providing a clear basis for comparing the performance of different AUV body configurations. These metrics also help in evaluating practical implications for control effort and energy consumption during various maneuvers.

Table 6 Calculated coefficients by GUI and [22]

Parameters	Cardenas et al.	Present value	Error %	Parameters	Cardenas et al.	Present value	Error %
$m - X_{\dot{u}}$	75.42	74.45	1.28	Y_{vv}	-130	-113.43	**12.74**
X_{uu}	-5.165	-5.33	-3.19	Y_R	51.78	65.35	**-26.20**
$m + X_{vr}$	74.2	72.92	1.72	N_{vv}	-11.25	-6.67	**40.71**
X_{rr}	16.7	15.47	7.36	N_{ur}	-41.9	-56.64	**-35.17**
$m - Y_{\dot{v}}$	145.5	145.72	-0.15	$N_{\dot{v}}$	6.548	5.47	**16.46**
$Y_{\dot{r}}$	5.775	5.47	5.2	$I_{zz} - N_{\dot{r}}$	31.51	39.48	**-25.29**
Y_{uv}	-135	-90.45	33	N_R	-32.94	-41.17	**-24.98**

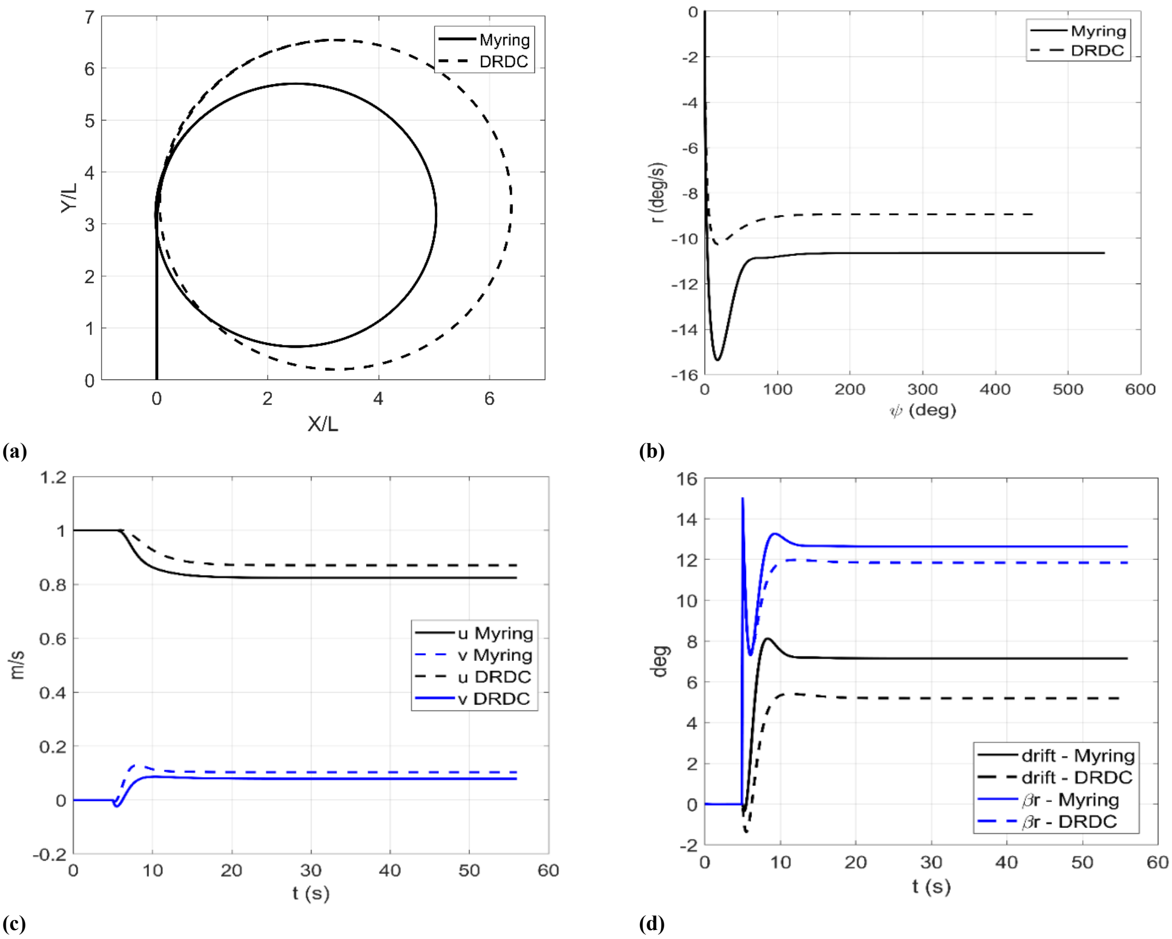

Fig. 9 Trajectory (a), yaw rate (b), axial velocities (c), body drift angle, and effective rudder angle (d) in the turning maneuver

6-2- Descending maneuver

In this section, the focus is on simulating depth changes for the AUV using the SUT-AUVSIM. During an endurance mission, the AUV must be able to change its operating depth as needed. Scenarios such as data acquisition, seabed profiling, and obstacle avoidance are conditions where the AUV initiates a depth change.

The descending maneuver for the AUV, with the specifications provided in Section 6.1, is simulated. The AUV starts at an initial depth of -1 meter and descends to a depth of -3 meters between seconds 5 and 80. After 80 seconds, the desired depth is returned to -1 meter. To maintain the AUV's depth position, a PD controller is used to adjust the rudder angle. The controller coefficients are selected to operate within an optimal range for each case. Throughout this maneuver, the propeller's rotational speed remains constant.

The results, demonstrated in Figure 10, indicate that the AUV changes its depth from -1 meter to -3 meters in 5.2 seconds. The axial velocities and body drift angle values during the maneuver are within normal range, and no instability in the behavior or velocities is observed. This simulation confirm that under the specified conditions and with a dive angle of 22 degrees, the AUV does not experience instability. The effective fin angle plot further validates that a maximum angle of 15 degrees for a 22-degree dive provides sufficient performance, ensuring that the AUV encounters no issues during the maneuver.

6-3- Helical maneuver

Due to the high endurance depth requirements in some AUVs, the descending maneuver may differ from the method presented in Section 6.2. In the previous section, for a depth change of 2 meters, the AUV displaces approximately 6.8 meters, which can become a significant distance for higher depths. Therefore, the helical maneuver is introduced to address this issue. Factors such as fin and rudder angles, mass, dive angle, body profile, and fluid properties can all be evaluated into the simulation. In this maneuver, the fins and rudders are deflected to their maximum angles, creating a three-dimensional helical path. Both the Myring and DARPA body profiles are used for this simulation. Initially, the AUV moves with 1 m/s, and in the self-propulsion conditions. The rudder is then turned to 15 degrees, and the fins are deflected to 10 degrees, and both simulations run for 75 seconds.

The results in Figure 11 show the output from the SUT-AUVSIM for simulating the helical maneuver for the Myring and DARPA profiles. The body drift angle significantly influences the effective attack angle of the rudder. However, the drift angle is not the only contributing factor; the yaw rate also plays a pivotal role. As the yaw rate increases, the induced drag in the surge motion also increases, leading to a greater reduction in forward velocity. Although the Myring body has a smaller turning radius, it experiences a greater velocity reduction compared to the DARPA body, despite both profiles having identical input conditions.

During the helical maneuver, the yaw rate plots indicate a noticeable drop in rotational velocity, suggesting that the vehicle requires additional control input to maintain the desired trajectory. This increase in control effort implies higher energy consumption, highlighting a trade-off between maneuverability and operational endurance. Considering these factors provides a more practical assessment of AUV performance, particularly when evaluating the efficiency of different hull configurations under complex maneuvers.

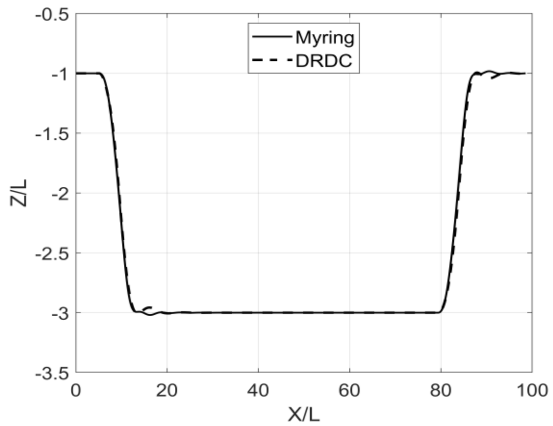

(a)

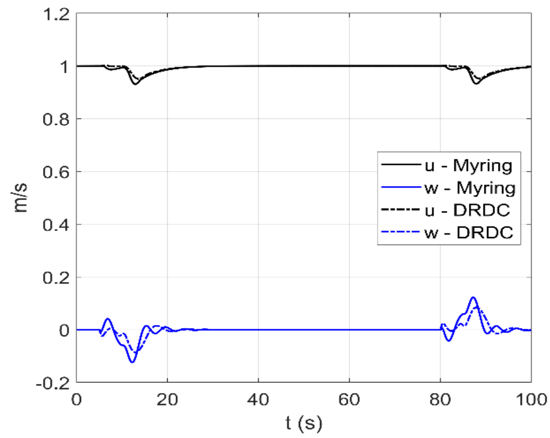

(b)

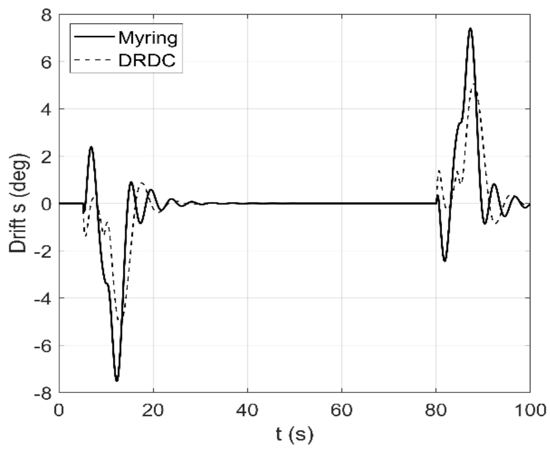

(c)

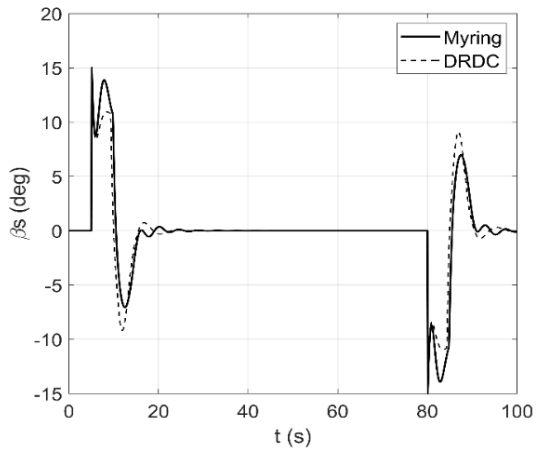

(d)

Fig. 10 Trajectory (a), axial velocities (b), body drift angle (c), and effective fin angle (d) in the descending maneuver

Table 7 Calculated coefficients by GUI and [22]

Maneuver	Tactical diameter (/L)		Depth change rate (/L) per 10 seconds		Steady time (s)	
	Myring	DRDC	Myring	DRDC	Myring	DRDC
Turning	4.91	6.23	-	-	15.78	18.6
Descending	-	-	2.03	2.09	-	-
Helical	4.63	5.15	2.1	2.78	18.44	28.81

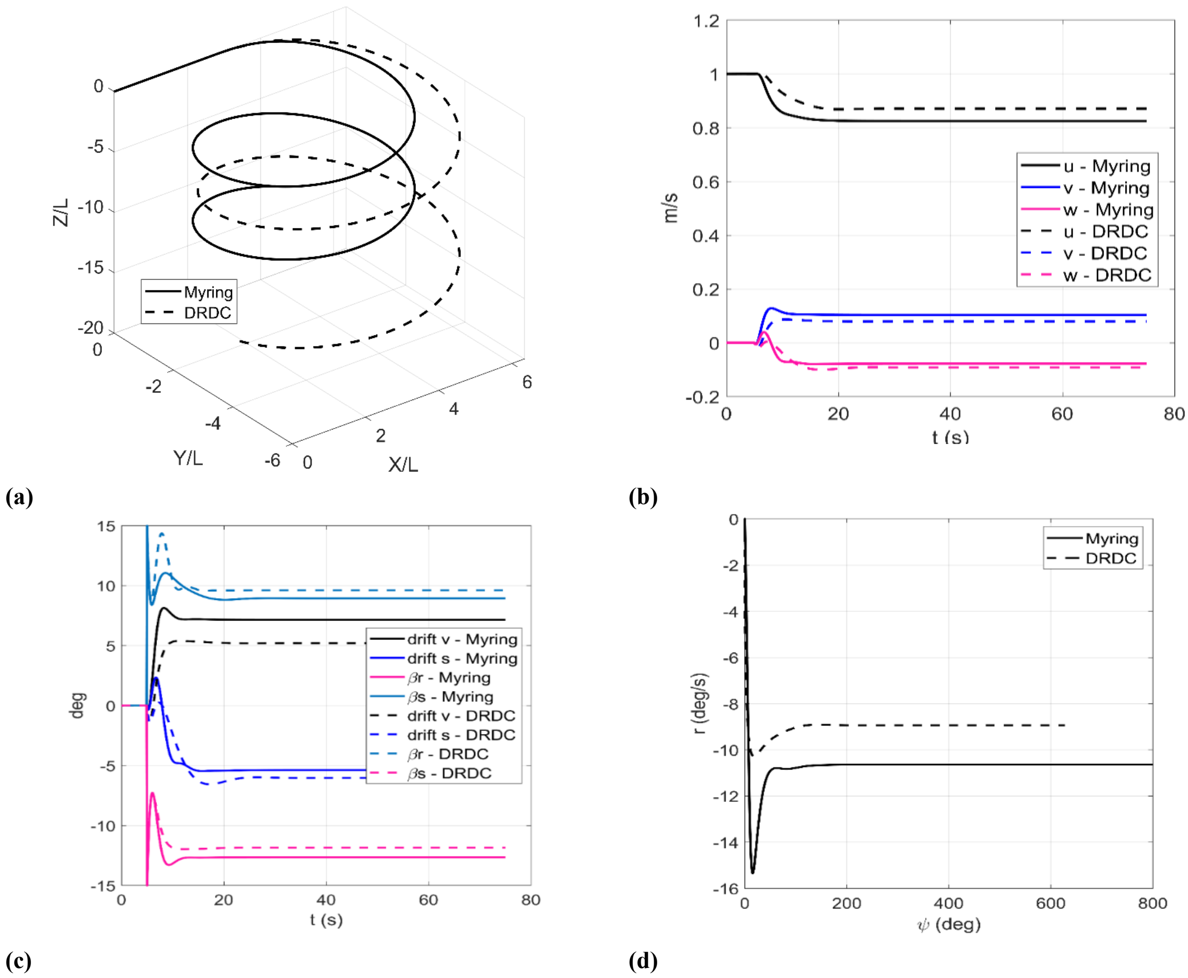

Fig. 11 Trajectory (a), axial velocities (b), body drift angle and effective fin angle (c), and yaw rate (d) in the helical maneuver

7- Conclusion

A practical GUI-based environment for maneuverability and dynamic analysis of marine vehicles can significantly reduce computational time. AUVs with torpedo-shaped bodies, due to their simple geometry, are particularly well-suited for such methods. Most AUVs have a torpedo-shaped body with four fins arranged in a C-type configuration, enabling the development of specialized programs tailored to these vehicles. The SUT-AUVSIM is a MATLAB GUI-based environment capable of calculating hydrodynamic derivatives using strip theory and performing 6-DOF maneuver modeling. The study demonstrated that the time required for dynamic modeling is significantly reduced for users. Additionally, since the calculations are based on user-defined inputs, it becomes easier to compare various concept designs, evaluate the impacts of specific parameters, and explore different geometric shapes in a short time. In turn, users can quickly assess how these factors influence the AUV's dynamics. Simulations of turning, descending, and helical maneuvers provide valuable insights into the AUV's performance and maneuverability. These simulations revealed that standard bodies with high block coefficients, such as DRDC, results in narrower maneuverability during turning maneuvers compared to the Myring body. This finding is crucial for control system design and obstacle avoidance. However, in the descending maneuver, the DRDC body exhibited better stability, attributed to its higher damping coefficient. It should be noted, however, that the method relies on potential flow assumptions, which may not fully capture nonlinear effects at higher speeds or complex flow regimes. This limitation may impact the accuracy of the results in some scenarios where more sophisticated CFD-based approaches would be necessary.

Acknowledgments
This work was conducted at the Sharif University of Technology using equipment from the Marine Engineering Research Center (MERC).

Ethics Approval
The scientific content of this article is the result of the authors' research and has not been published in any Iranian or international journal.

Conflict of Interest
This article includes some results from the authors. There are no other conflicts of interest to declare.

Funding Statement
This research has received no specific grant from any funding agency in the public, commercial, or not-for-profit sectors.

Author Contributions
A. Hasanvand was responsible for conceptualization, methodology, software, and validation of the results. The original draft of the manuscript was written by A. Hasanvand, and all authors participated in the review and editing process. M. S. Seif provided supervision and project administration.

References

[1] Zhou, J., Si, Y. and Chen, Y., 2023. A review of subsea AUV technology. Journal of Marine Science and Engineering, 11(6), p.1119. doi: 10.3390/jmse11061119.

[2] Kot, R., 2022. Review of collision avoidance and path planning algorithms used in autonomous underwater vehicles. Electronics, 11(15),p.2301. doi: 10.3390/electronics11152301.

[3] Hasanvand, A. and Seif, M.S., 2024. Development of state space models for underwater gliders equipped with embedded actuators in vertical and horizontal planes. Ocean Engineering, 309, p.118344. doi: 10.1016/j.oceaneng.2024.118344.

[4] Santiesteban Cos, R., Carretero, J.A. and Sensinger, J., 2022. Modelling of a Hydrodynamically Actuated Manipulator Based on Strip Theory. In Multibody Mechatronic Systems: MuSMe 2021 7 (pp. 171-180). Springer International Publishing.

[5] Lambert, W., Miller, L., Brizzolara, S. and Woolsey, C., 2022, October. A strip theory and CFD informed lumped parameter model for near-surface underwater vehicle maneuvering. In OCEANS 2022, Hampton Roads (pp. 1-7). IEEE. doi: 10.1109/OCEANS47191.2022.9976993.

[6] Eng, Y.H., Chin, C.S. and Lau, M.W.S., 2014. Added mass computation for control of an open-frame remotely operated vehicle: Application using WAMIT and MATLAB. Journal of Marine Science and Technology, 22(4), pp.405-416. doi: 10.6119/JMST-013-0313-2.

[7] Fossen, T.I., 2011. Handbook of marine craft hydrodynamics and motion control. John Wiley & Sons.

[8] Seif, M.S. and Hasanvand, A., 2021. Investigating the geometry and control surface of AUV robots on hydrodynamics performance. Journal of Marine Engineering, 17(33), pp.53-64.

[9] Gutnik, Y., Avni, A., Treibitz, T. and Groper, M., 2022. On the adaptation of an auv into a dedicated platform for close range imaging survey missions. Journal of Marine Science and Engineering, 10(7), p.974. doi: 10.3390/jmse10070974.

[10] Hasanvand, A. and Seif, M.S., 2024. Investigation the effect of length-to-diameter ratio on six-DOF helical and zigzag maneuvers of the SUT glider with internal actuators. Ocean Engineering, 295, p.116819. doi: 10.1016/j.oceaneng.2024.116819.

[11] Allotta, B., Costanzi, R., Pugi, L. and Ridolfi, A., 2018. Identification of the main hydrodynamic parameters of Typhoon AUV from a reduced experimental dataset. Ocean Engineering, 147, pp.77-88. doi: 10.1016/j.oceaneng.2017.10.032.

[12] Randeni P, S.A.T., Forrest, A.L., Cossu, R., Leong, Z.Q., Ranmuthugala, D. and Schmidt, V., 2018. Parameter identification of a nonlinear model: replicating the motion response of an autonomous underwater vehicle for dynamic environments. Nonlinear Dynamics, 91, pp.1229-1247. doi: 10.1007/s11071-017-3941-z.

[13] Nouri, N.M., Valadi, M. and Asgharian, J., 2018. Optimal input design for hydrodynamic derivatives estimation of nonlinear dynamic model of AUV. Nonlinear Dynamics, 92, pp.139-151. doi: 10.1007/s11071-017-3611-1.

[14] Ji, D., Wang, R., Zhai, Y. and Gu, H., 2021. Dynamic modeling of quadrotor AUV using a novel CFD simulation. Ocean Engineering, 237, p.109651. doi: 10.1016/j.oceaneng.2021.109651.

[15] Hong, L., Fang, R., Cai, X. and Wang, X., 2021. Numerical investigation on hydrodynamic performance of a portable AUV. Journal of Marine Science and Engineering, 9(8), p.812. doi: 10.3390/jmse9080812.

[16] Tao, Y., Li, X., & Wang, P. (2024). CFD-based hydrodynamic performance investigation of autonomous underwater vehicles: A survey. Ocean Engineering, 305, 117911. doi: 10.1016/j.oceaneng.2024.117911.

[17] Zhang, Q., Liu, H., & Zhao, J. (2024). Review of Computational Fluid Dynamics Analysis in Biomimetic Applications for Underwater Vehicles. Biomimetics, 9(2), 79. doi: 10.3390/biomimetics9020079.

[18] Zhou, G., Xiang, X. and Liu, C., 2023. Parameter identification and model prediction path following control of underactuated AUV: Methodology and experimental verification. Control Engineering Practice, 141, p.105729. doi: 10.1016/j.conengprac.2023.105729.

[19] Hasanvand, A. and Seif, M.S., 2021. Investigating the geometry and control surface of AUV robots on hydrodynamics performance. Journal of Marine Engineering, 17(33). doi: 10.1016/j.oceaneng.2024.116819.

[20] Hasanvand, A. and Seif, M.S., 2024a. Adaptive path-following control for high-underactuated underwater glider under hydrodynamic coefficient uncertainties. Journal of Marine Science and Technology, 29(4), pp.1000-1017. doi: 10.1007/s00773-024-01032-0.

[21] Yang, L., Xiang, X., Kong, D. and Yang, S., 2024. Small Modular AUV Based on 3D Printing Technology: Design, Implementation and Experimental Validation. Brodogradnja: An International Journal of Naval Architecture and Ocean Engineering for Research and Development, 75(1), pp.1-16. doi: 10.21278/brod75104.

[22] Cardenas, P. and de Barros, E.A., 2019. Estimation of AUV hydrodynamic coefficients using analytical and system identification approaches. IEEE Journal of Oceanic Engineering, 45(4), pp.1157-1176. doi: 10.1109/JOE.2019.2930421.